Flow Physics and Mixing of a Confined Impinging Jet Mixer

by

Yue Hao

A thesis submitted to The Johns Hopkins University in conformity with the requirements for the degree of Master of Science in Engineering.

Baltimore, Maryland

May 2019

Abstract

Confined Impinging Jet Mixers (CIJM) are employed widely in chemical processes that requires fast mixing such as precipitation and production of nanoparticles because of their ability to provide rapid mixing at small-scales. In this mixing device, two jets from opposite sides directly impinge on each other. This forms thin shear layers which immediately breaks down into small structures thereby enabling effective mixing of the species transported by each jet. Interaction of the shear layers with the inner walls can induce self-sustained oscillation of the shear layer. The present study is focused on investigating the flow physics, especially the instability of the shear layer and self-sustained oscillation generated by the impinging jet and the enhancement of mixing of these devices. The study employs direct numerical simulation (DNS) with a sharp interface immersed boundary method and mixing is modeled via the modeling of passive scalars. The flow structures are visualized via the vortex topology, turbulent kinetic energy and other variables, and mixing is quantified by defining the uniformity and cross correlation of chemical species (non-

reacting as well as reacting). Results are analyzed to gain insight into the effect of Reynolds number on the effectiveness of mixing, which is a key operational parameter for these devices. Based on our analysis, we propose and test a novel axisymmetric CIJM that is designed for improved mixing performance.

Primary Reader and Advisor: Jung-Hee Seo

Secondary Reader: Rajat Mittal

Acknowledgments

I am sincerely grateful to Prof. Mittal and Prof. Seo for providing me this opportunity to work in their group in the past one and half years. Prof. Mittal and Prof. Seo provided me with lots of guidance on research topic and training on my research skills. This experience is a start for my research on computational fluid dynamics and provided me a solid foundation for my Ph.D. research.

I would like to thank my group mates, Zhuoyu Zhou, Chi Zhu, Aaron Rips, Karthik Menon, Shantanu Bailoor and Chuanxin Ni. The discussion with them is really inspiring.

Contents

List of Tables

List of Figures

Chapter 1

Introduction

Effective mixing is the key component in the processing and manufacturing of products such as pharmaceuticals, pesticides and cosmetics. Mixing via flow turbulence has the following advantages: first, turbulence can help flow and transported species break down into small scales, leading to a more uniform mixing; second, turbulence can help the transported species achieve homogeneity rapidly. For chemical reaction systems that require uniform production, rapid mixing is crucially important because if the mixing speed is slow, the mixing and reaction processes will be coupled resulting in non-uniform product. Turbulent mixing can be introduced by T connectors [1], Tesla mixers and herring-bone mixers [2], coaxial jet mixers [3], [4], Confined Impinging Jet Mixer (CIJM) [5], [6] and multi-inlet vortex mixers (MIVM) [7].

Confined Impinging Jet Mixers (CIJMs) are widely used in chemical pro-

cesses that require fast and intensive mixing, and can be used for injecting reactants, and as opposed jets burners [8] and precipitators [9]. A CIJM contains two or more impinging jets and a mixing chamber. Liquid chemical solution are injected as jets into the confined chamber and the jets impinge inside the chamber. Fluctuating flow pattern in the chamber can result in high quality mixing of the multiple chemical species and the mixed species flow through the chamber towards the outlet. [10]

The study of CIJM has been driven by extensive industrial need. The initial work of Prudhomme et al. [5]drew significant interest into the mixing and reaction of nanoparticles using CIJM. Santos et al. [11] introduced the CIJM into the production of polyelectrolyte complex nanoparticles in a continuous and scalable manner. Nikoubashman et al. [12] implemented the CIJM to achieve rapid micromixing of polymers in solution with a nonsolvent for the directed assembly of soft nanoparticles, showing this mixing mechanism is highly promising for the mass fabrication of uniformly sized colloidal particles, using a wide variety of polymeric feed materials.

Although the CIJM has been widely used in industry, the understanding of the flow physics and mixing quality of the CIJM is still limited. Most studies focus on the visualization of flow field experimentally or computationally, and also the investigation of the mixing quality from different aspects, such as mixing uniformity, mixing length scale, and mixing time scale.

Tucker and Suh [13] used flow visualization to show that the flow in directly opposed jets transitions at a Reynolds number of approximately 140 based on jet velocity and inlet diameter. Wood et al [14] investigated the flow field of CIJM experimentally and numerically. They captured the Strouhal number of lateral velocity as a function of Reynolds number and observed a low frequency fluctuation pattern of the flow at Strouhal number normalized with inlet jet diameter and inlet velocity of 0.01 approximately. Unger and Muzzio [15] implemented laser-induced fluorescence (LIF) technique to visualize the concentration field of chemical species injected from one side of CIJM, and offered a technique to better quantify the mixing. Johnson and Wood [10] introduced the concept of self-sustained oscillation, quantified the fluctuation frequency by using spectral analysis on the data of LDA measurement. Their result is similar to the result of Tyagi [14] in that the Strouhal number of lateral velocity is of the order of 0.01. Santos et al [16] visualized the flow field experimentally by PIV technique, and quantified the intensity of turbulence by calculating the root-mean-squate (RMS) and probability function (PDF) of velocity as a function of Reynolds number. Icardi et al [17], Santos et al [18] and Marchisio [19] also performed LES for the simulation of flow field of CIJM.

The intensity of segregation (IoS) , which is defined as the spatial RMS of the concentration of chemical species, is often used to quantify the uniformity of the distribution of the chemical species. Unger et al [14] and Fonte et al

[20] demonstrated that the CIJM has very good mixing quality in terms of IoS. The IoS decreased with Reynolds number, and is always less than 0.1. The mixing length scale is also important to quantify the mixing quality but currently there is no clear definition of the mixing length scale. and most of the definitions are based on analytical models. Lee et al [21], Baldyga and Bourne [22], Tucker et al [13] separately made prediction of mixing length scale as a function of Reynold number. Fonte et al [20] demonstrated the model of Lee [21] et al is most reliable based on their experimental result. Currently, there is no common metric to quantify the mixing length scale, but one way is to quantify it computationally by capturing the peak wavelength of the spatial velocity spectrum. [23]

In the present work, we investigated the flow physics of CIJM by direct numerical simulation (DNS) and analyzed the vortex structures and the statistics of the flow field to quantify the turbulence. While intensity of segregation has been used widely for the quantification of mixing uniformity, this metric is not good enough to quantify the mixing of multiple chemical species. This is because the uniformity of distribution of one chemical species does not necessarily imply that it is well mixed with the other. Only when the concentration of each chemical species is similar at each location, can it be claimed that good mixing has been achieved. In addition, mixing quality is not the only concern of CIJM when it is used for chemical reactions. The uniformity of the product is

of great concern for processes such as drug production, since nonuniform product size or composition can result in variation in drug efficacy. [11] The mixing quality is also investigated by quantifying the uniformity and the cross correlation of chemical species spatial distribution. The uniformity of the product of possible chemical reaction is also investigated by introducing the residence time in the CIJM.

Chapter 2

Model Configuration

2.1 Geometry

The confined impinging jet mixer consists of two opposed circular cylinder injector tubes (with diameter d), and a cylindrical mixing chamber (with diameter D). The injectors are placed close to the top wall of the mixing chamber with the distance to the top wall designated as H. The specific dimension of the geometry used in the present study is extracted from the experimental literature [20]. Figure 2.1 (a) shows the 3D view of the geometry and Figure 2.1 (b) shows the frontal view and dimension of the Geometry. The characteristic length scale is chosen to be d, the diameter of the injector, and the characteristic velocity scale is the average injector velocity V_{in}. The characteristic time scale is therefore defined as $t* = d/V_{in}$. The coordinate system employed in

our description is also shown in Figure 2.1 and we note that the jets are directed along the x-direction and the axis of the mixing chamber and the outlet is aligned along the y-direction.

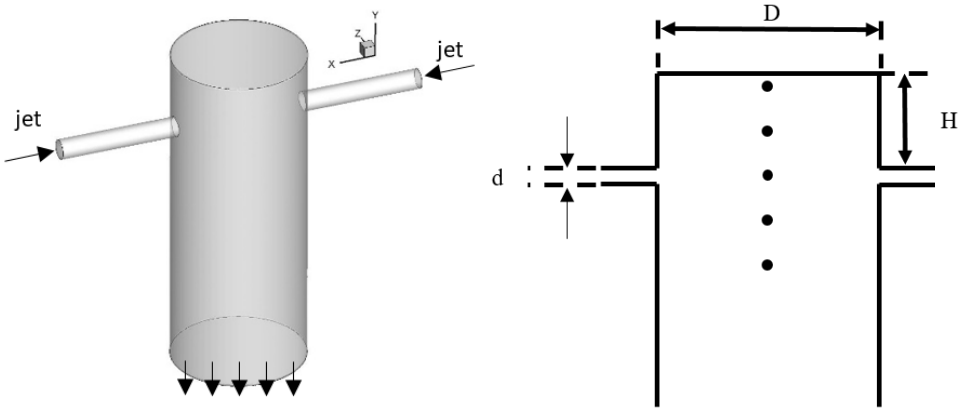

Figure 2.1: (a) 3D view of Computational Geometry. (b) Frontal View and Dimension of Geometry.

2.2 Numerical Methods

Flow simulations are performed by solving the incompressible Navier-Stokes equations:

$$\nabla \cdot \vec{\mathbf{u}} \tag{2.1}$$

$$\frac{\partial \vec{\mathbf{u}}}{\partial t} + \nabla \cdot \vec{\mathbf{u}}\vec{\mathbf{u}} = -\frac{\nabla p}{\rho} + \mu \nabla^2 \vec{\mathbf{u}} \tag{2.2}$$

where $\vec{\mathbf{u}} = (u, v, w)$ is the fluid velocity vector, p is the pressure, ρ and ν

are the density and kinematic viscosity of water. The equation is solved by the projection method [24] on the Cartesian grid and a sharp interface immersed boundary method [25] [26] is employed to represent the effect of the boundaries. The number of grid points in the x, y, and z directions are 380, 292 and 164 (total Grid point 18,197,440). The resolution is chosen based on the grid convergence study (see appendix A). A fixed time-step size of $\Delta t = 0.01d/V_{in}$ is employed and the maximum CFL number ($u\Delta t/\Delta x$) is kept around 0.31 to ensure the stability of the simulation. Dirichlet boundary conditions ($u = V_{in}$) is employed at the inlet, Neumann boundary condition of zero velocity gradient is employed at the outlet, and a noslip boundary condition is employed at the inner wall of the device. The flow simulation is performed on the MARCC (Maryland Advanced Research Computing Center) cluster using 256 CPU cores and approximately 70 hours are required for each case running 400 non-dimensional time $t*$. The jet Reynolds number $Re = V_{in}d/\nu$ is a key variable in the analysis of the CIJM and is varied over a small range.

To evaluate the mixing quality of CIJM, two passive transported scalars are released from the two jets, and the mixing quality of the two scalars are investigated. The concentration fields of these scalars are obtained by solving the following convection-diffusion equation.

$$\frac{\partial c_i}{\partial t} + \vec{\mathbf{u}} \cdot \boldsymbol{\nabla} c_i = \frac{1}{Re \cdot Sc} \boldsymbol{\nabla}^2 c_i; i = 1, 2 \tag{2.3}$$

where c_i is the concentration of i^{th} scalar, $\vec{u}$ is the velocity of fluid, *Re* is Reynolds number of the fluid, and *Sc* is Schmidt number of the solution.

To investigate the influence of Schmidt number on the mixing, a high Schmidt number of 100 and a low Schmidt number of 1 is used in this study.

Chapter 3

Confined Impinging Jet Mixer

The simulations are performed with jet Reynolds numbers of 200, 600 and 1000 and the simulation data analyzed to gain insight into the flow dynamics and mixing performance. Chemical species are represented by scalar concentrations, and Schmidt numbers of 100 and 1 are studied separately. The discussion in this section are based on nondimensional numbers and all the values are scaled with length scale d and velocity scale V_{in}.

3.1 Vortex Dynamics

Figure 3.1 - 3.3 respectively shows the development of, the second invariant of the velocity gradient (Q) in 3D view and z-direction vorticity in side view slice (the location of the slice is shown in Figure 2.1 (b) of confined impinging

jet mixer) for Re=200, Re=600 and Re=1000 case.

The overall flow patterns in the CIJM with different Reynolds number are similar. At the beginning, the two jets directly impinge on each other and a vortex core and a thin disk like shear layer is formed at the impinging center. The vorticity stripe shown by sub figures 3.1 - 3.3 (b) and (d) is the shear layer in that slice. Shortly after, the disk like shear layer starts flapping, twisting and deforming, and small-scale vortical structures are also radiated from the impinging center towards the radial direction of the impinging plane.

The experimental result of Fonte et. al. [20] also shows an impinging jet induced shear layer, the oscillation of the shear layer, and the vortex shedding induced by the shear layer oscillation, which is similar with the simulation result.

The instability of the flow in the CIJM has several potential mechanisms. First, the shear layer of the impinging jet has intrinsic instabilities, especially at high Reynolds numbers and this leads to vortex roll up in the downstream radial direction of the impinging plane. Second, the interaction of shear layer and the inner wall of the device can also induce the formation of vortex structures. Third, vortex structures generated by the interaction of the jet shear layer and the wall can feed perturbations back into the shear layer and even the main jet, inducing a larger amplitude of fluctuation, and consequently creating more vortical structures. The two physical processes, interaction with the

inner wall and the interaction back to the shear layer of the jet, are completely coupled with each other, making the flow pattern more and more unstable. Another interesting phenomenon is that the impinging point, which is defined by the point that has the lowest velocity magnitude along the $x$direction centerline of the device, also exhibits large scale movements. The first source of this movement is that although the device is symmetrical in xdirection, the transport of vortex perturbations can generate small differences on the left and right sides of the mixer, and this could initiate the movement of the impingement point. The movement of the impingement point away from the center leads to a stronger asymmetry of the vortex distribution and can continuously induce the movement of the impingement point. The second source is the interaction between the vortical structures and the main jets. This interaction is quite strong and it can induce a sudden shift of the impinging point, as shown in Figure 3.2(b) and Figure 3.3 (b).

Comparing the flow patterns of each Reynolds number cases, the most obvious difference is that the vortical structure has a smaller scale and the flow pattern is more unstable with an increase in the Reynolds number. This means that for the larger Reynolds number case, the interaction with the shear layer and the main jet is affected by the smaller scale structures.

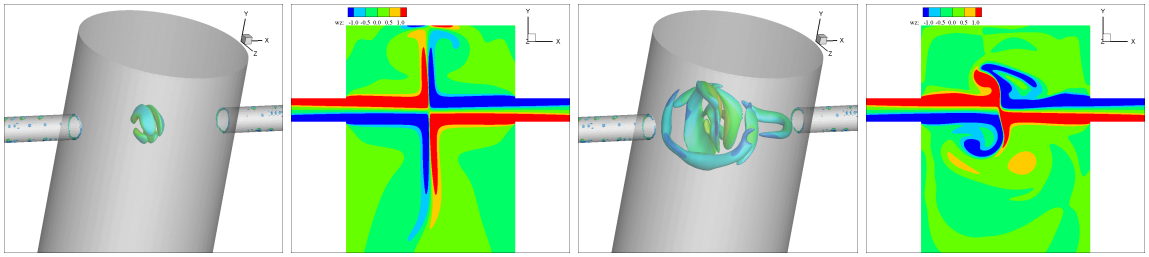

Figure 3.1: Flow Field of Re = 200 case. (a) Q-vortex at t*=300. (b) ω_z at t*=300. (c) Q-vortex at t*=354. (d) ω_z at t*=354.

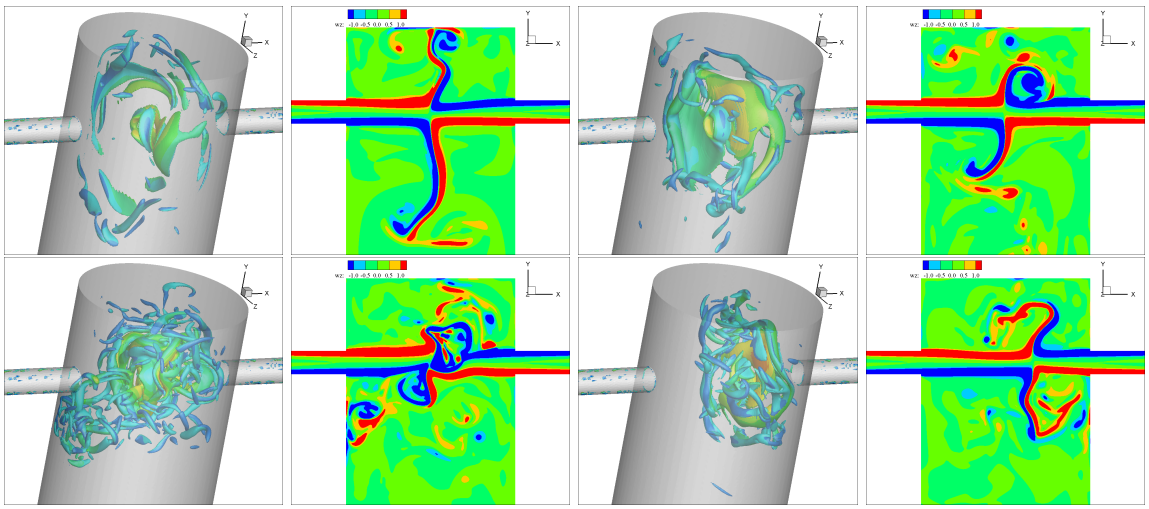

Figure 3.2: Flow Field of Re = 600 case. (a) Q-vortex at t*=117. (b) ω_z at t*=117. (c) Q-vortex at t*=165. (d) ω_z at t*=165. (e) Q-vortex at t*=271. (f) ω_z at t*=271. (g) Q-vortex at t*=365. (h) ω_z at t*=365.

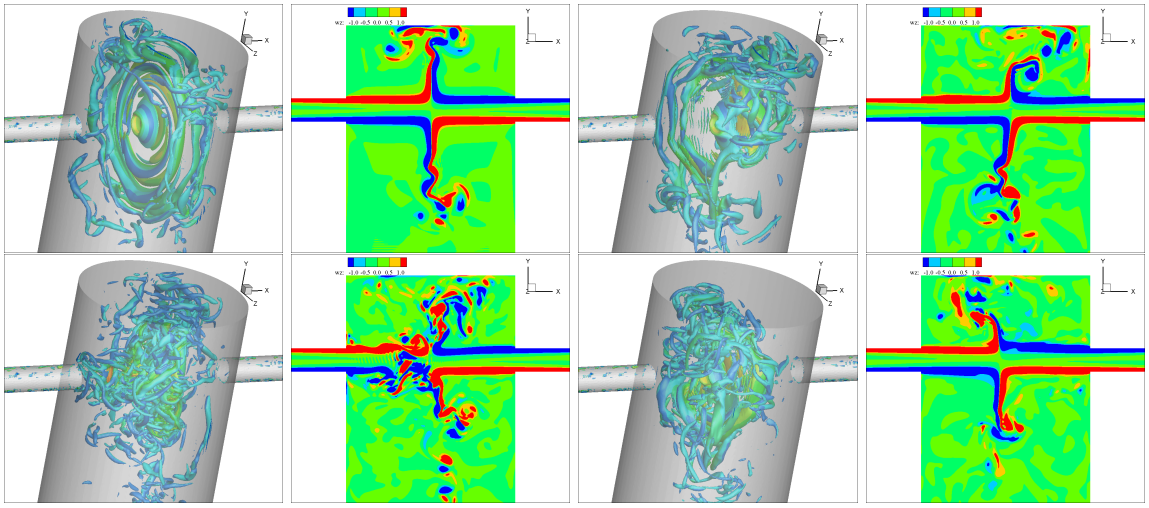

Figure 3.3: Flow Field of Re = 1000 case. (a) Q-vortex at t*=23. (b) ω_z at t*=23. (c) Q-vortex at t*=235. (d) ω_z at t*=235. (e) Q-vortex at t*=310. (f) ω_z at t*=310. (g) Q-vortex at t*=346. (h) ω_z at t*=346.

3.2 Flow Statistics

To better evaluate the overall behavior of the flow field, the statistics of the flow field, such as average flow field and the RMS fluctuations of the velocity are extracted. First, the time evolution of the flow is divided into several periods based on the movement of the impinging point. As mentioned in section 3.1, the impingement point can exhibit sudden shifts over a large and stochastic time-scale. Thus the flow periods (or stages) are defined by the duration between the sudden shifts. For example, the definition of flow period for Re=600 case is shown in Figure 3.4, and the detailed time range of the flow stage and the position of the impingement point for each flow stage are shown in Table

3.1.

Another interesting phenomenon is that the movement of impingement point is the largest in the Re = 600 case, even larger than Re = 1000 case, as shown in Figure 3.4. A possible reason is that as shown in Figure 2-4 and discussed in section 3.1, the interaction between the vortical structures and the main jet for Re = 600 case is driven by a large scale vortex. For Re = 1000 case, however, the large scale vortex already breaks down into smaller scales before it interacts with the shear layer and the main jet. Consequently, the intensity of interaction of Re = 600 case is stronger and this results in the larger amplitude of the movement of the impingement point.

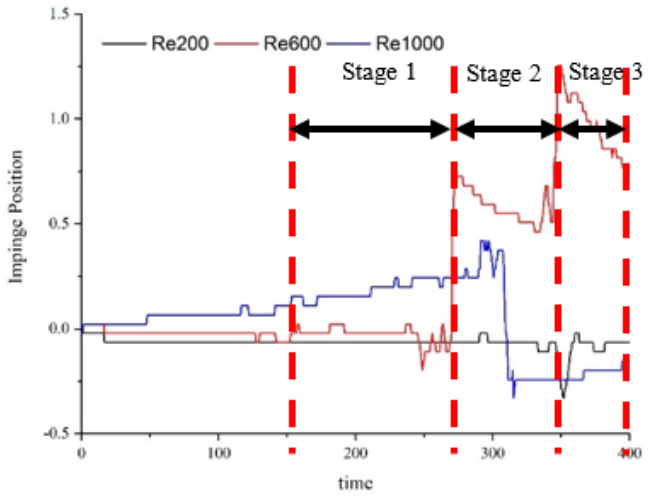

Figure 3.4: Movement of impingement point.

Table 3.1: Movement of impingement point .

Re	Stage Name	impingement point	Time Start	Time End
200	Stage 0	0.000	0.00	280.67
	Stage 1	-0.066	280.67	400.00

600	Stage 0	0.000	0.00	120.67
	Stage 1	0.022	120.67	246.67
	Stage 2	0.590	270.67	346.67
	Stage 3	0.947	352.00	400.00
1000	Stage 0	0.000	0.00	153.33
	Stage 1	0.211	153.33	306.67
	Stage 2	-0.222	310.67	400.00

Figure 3.5 - 3.7 shows the time-averaged flow field of velocity magnitude and turbulent kinetic energy in the CIJM with different Reynolds numbers on the side-view plane and the top-view plane at the last flow stage shown in figure 3.4.

Comparing the flow patterns of Re = 200, Re = 600 and Re = 1000 case, the overall flow pattern is similar except for the impingement point location. The two jets are impinging and the fluid particles are flowing towards radial direction from the impinging center. The large scale fluctuation of the flow field is mainly driven by the flapping of the impinging disk. The spatial range and amplitude of flapping can be viewed by the region with high turbulent kinetic energy (TKE). The definition of TKE is shown as follows:

$$TKE = \frac{1}{2}(\overline{(u')^2} + \overline{(v')^2} + \overline{(w')^2}) \tag{3.1}$$

For all the cases, the flapping region is a fanshaped region in the 2D slice. Focusing on the region with high TKE where TKE > 0.2, the spatial range of the flapping of Re = 200 case is smaller than at Re = 600 and Re = 1000,

while two latter cases are similar. Also, for Re = 600 case, the high TKE region where TKE > 0.4, shown as color red (red) is occupying not only the flapping region, but also the impinging center. The reason is that the movement of impingement point for Re = 600 case is the largest among all the cases, making the fluctuation of velocity at the impingement point generates high TKE.

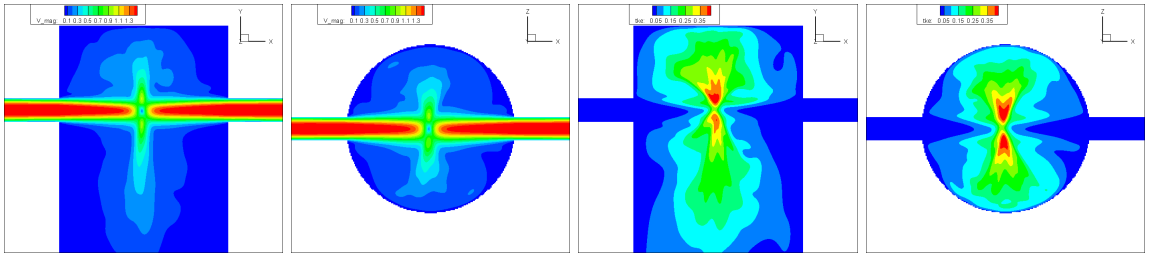

Figure 3.5: Statistical Flow Field of Re = 200 case. (a) Velocity magnitude at Z=0 slice. (b) Velocity magnitude at Y=0 slice. (c) TKE at Z=0 slice. (d) TKE at Y=0 slice.

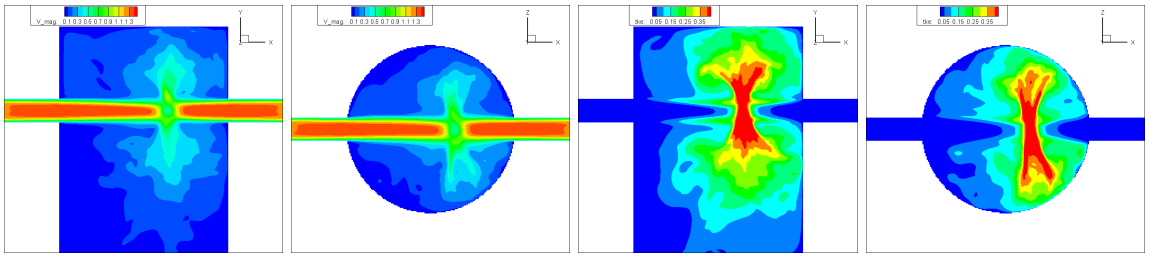

Figure 3.6: Statistical Flow Field of Re = 600 case. (a) Velocity magnitude at Z=0 slice. (b) Velocity magnitude at Y=0 slice. (c) TKE at Z=0 slice. (d) TKE at Y=0 slice.

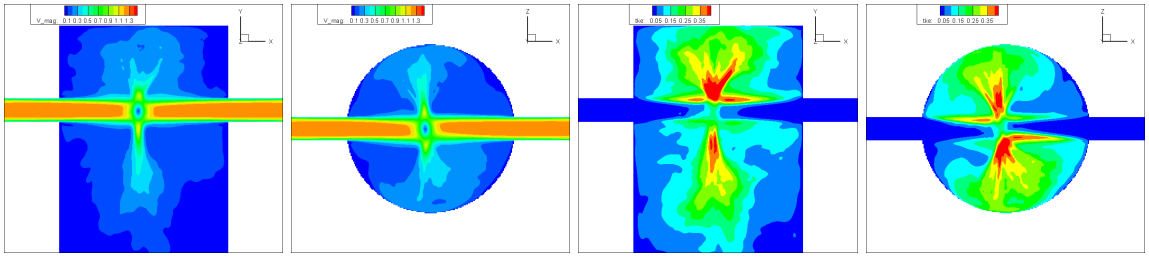

Figure 3.7: Flow statistics for the Re = 1000 case. (a) Velocity magnitude at Z=0 slice. (b) Velocity magnitude at Y=0 slice. (c) TKE at Z=0 slice. (d) TKE at Y=0 slice.

Figure 3.8 and Figure 3.9 show the distributions of the velocity magnitude and turbulent kinetic energy along the central axis of the CIJM. For each flow stage at each Reynolds number, the distributions of the velocity magnitude are similar; the velocity magnitude at the impingement point (Y=0) is very low, the velocity magnitude reaches peak value at half way down stream and decreases and reaching the minimum at the outlet of CIJM.

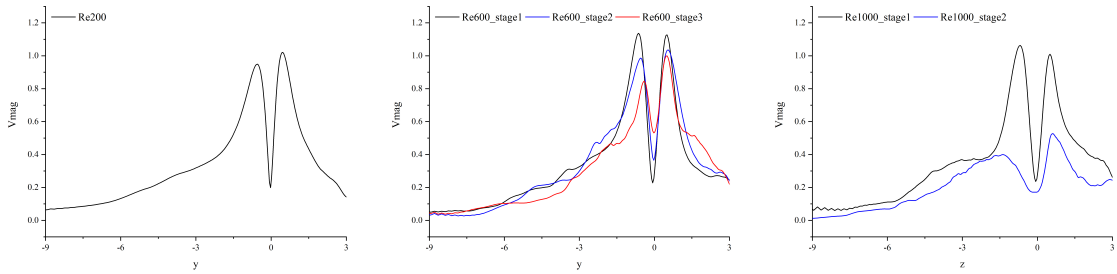

Figure 3.8: Velocity magnitude along y-center line (a) Re = 200. (b) Re = 600. (c) Re = 1000.

The distribution of turbulent kinetic energy is similar to the distribution of the velocity magnitude. The TKE reaches the peak value near the impingement point but shows the notch at the impingement point. In addition, the

peak of TKE near the top wall is higher than the peak of TKE at the downstream. This indicates that the confinement with the top wall can contribute to the additional instability of the flow.

Comparing the TKE distributions of all Reynolds number cases, the amplitude of TKE for Re = 600 and Re = 1000 cases are similar but they are higher than the Re = 200 case, which is consistent with the result shown in Figure 3.5 - 3.7. Also, note that the peak of the TKE appeared in stage 3 of the Re = 600 case originates from the movement of the impingement point.

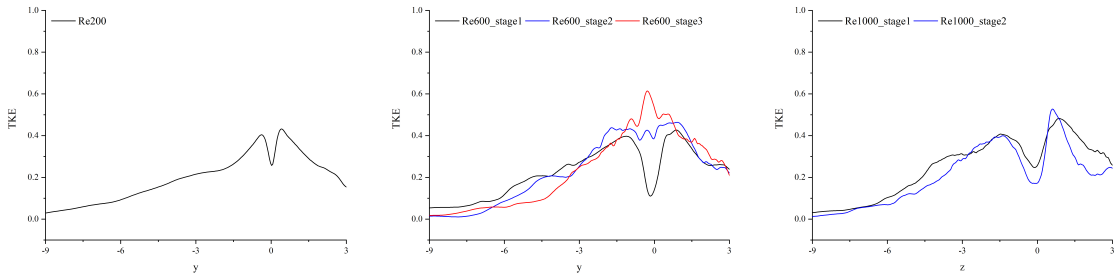

Figure 3.9: TKE along Y center line (a) Re = 200. (b) Re = 600. (c) Re = 1000.

3.3 Mixing Quality

The mixing quality is evaluated by two metrics. The first metric is the spatial uniformity of the concentration of the scalar 1 or 2, as defined by the following equation:

$$MI1 = 1 - \sqrt{\frac{\iint C(\vec{\mathbf{x}})^2 dA}{\iint dA}} \tag{3.2}$$

where C is the concentration of the scalar 1 or 2. This metric evaluates how uniformly the solution is distributed. This metric was used in previous studies, through an intensity of segregation index, which is $(1 - MI1)$ [15], [20].

The second metric is the cross-correlation of solution concentration 1 and solution concentration 2, defined as the following equation.

$$MI2 = \frac{\overline{C_1'(x) \cdot C_2'(x)}}{\sqrt{\overline{C_1'(x)^2} \cdot \overline{C_2'(x)^2}}} \tag{3.3}$$

where $C_1'(x)$ and $C_2'(x)$ are the spatial fluctuating value of solution concentration at each y direction slice of CIJM, defined as $C_1'(x) = C_1(x) - \overline{C_1(x)}$, and $MI2$ is scaled by the product of the spatial RMS of scalar concentrations 1 and 2. This metric shows how similar the distribution of the two concentration is within the volume of the mixer. The more similar these concentrations, the less difference there is of concentration at a position, and better the mixing. This metric is better than the first one to quantify mixing in a binary mixture.

The mixing indices are evaluated on each y-direction slice of the device, as shown in the blue slice plane in Figure 3.10.

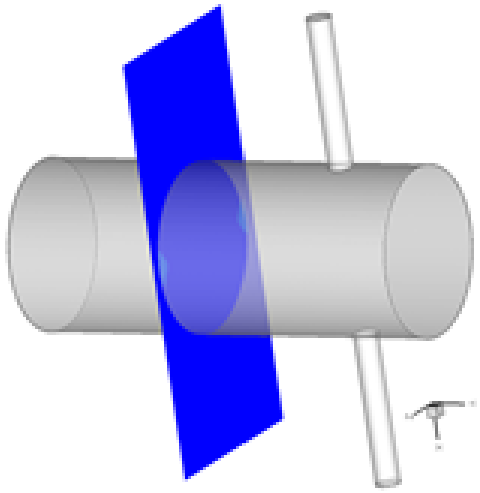

Figure 3.10: Y-direction slice.

Figure 3.11 and Figure 3.12 respectively shows the $MI1$ of the CIJM for each yslice of the scalars with Schmidt numbers of 100 and 1. The result of each flow stage of each Reynolds number case is presented. It can be observed from Figure 3.11 that for all flow stages of each Reynolds number cases, CIJM achieves good mixing, with $MI1 > 0.98$. In addition, good mixing is reached at a close position of the impinging plane, this indicates that CIJM is a very good mixer. This is inline with the previous study the result of Unger et al [15], and Fonte et al [20] showing the intensity of segregation are in the order of 0.05, which mixing index 1 of around 0.95.

Also, comparing different flow stages mixing index 1 of each Reynolds number case, the first flow stage always showing better mixing. The reason is that for the first stage, the impinging center is still at the center of impinging plane,

and the eccentric of impingement point of following flow stages can create non-uniformity of the distribution of solution concentration, and decrease the mixing index 1.

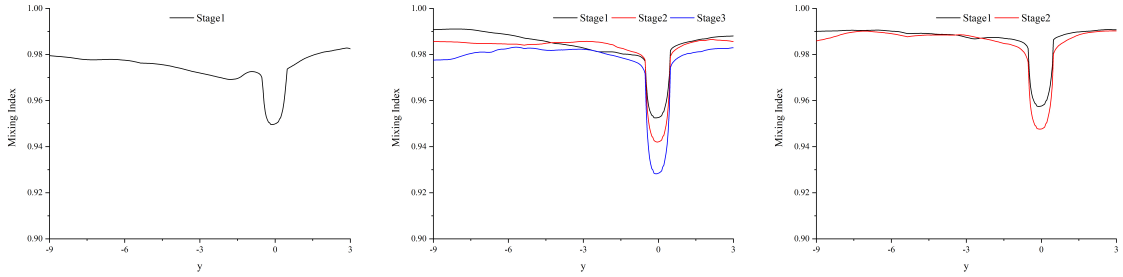

Figure 3.11: Plots of $MI1$ which depicts scalar uniformity for Sc = 100. (a) Re = 200. (b) Re = 600. (c) Re = 1000.

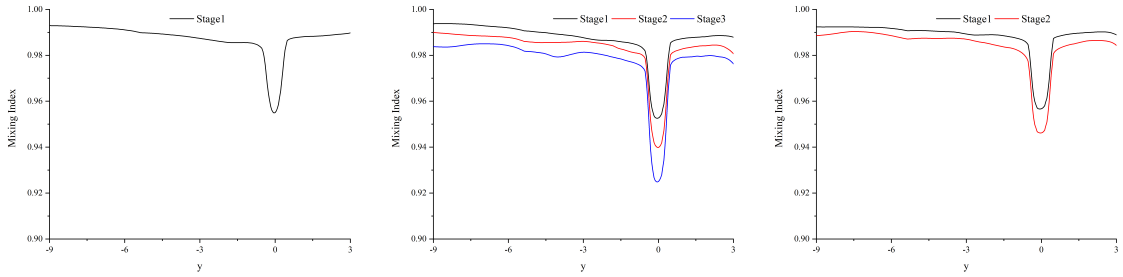

Figure 3.12: Plots of $MI1$ which depicts scalar uniformity for Sc = 1. (a) Re = 200. (b) Re = 600. (c) Re = 1000.

For the low Schmidt number cases (Sc = 1), the development of mixing index is very similar with cases with Sc = 100, but overall the mixing index is higher than the cases with high Schmidt number. The reason is that, at low Schmidt number case, higher diffusion improves the uniformity of the solution concentration and increases the mixing index.

Figure 3.13 and Figure 3.14 respectively shows $MI2$ for a Schmidt numbers

of 100 and 1. The results of each flow stage of each Reynolds number case are presented. It is observed from Figure 3.13 that in terms of the cross correlation of scalar concentration 1 and 2, better mixing is achieved at higher Reynolds numbers (Re = 600 and Re = 1000). However, for the Re = 200 case, $MI2$ is lower than 0, indicating that the concentrations of the two scalars are negatively correlated. This indicates that for Re = 200 case, even though the uniformity of each scalars is good, the mixing of the two is quite non-uniform. In addition, the mixing quality of flow stage 1 (where impingements occurs on the center) is better than the following stages where the impingement points moves significantly off-cente.

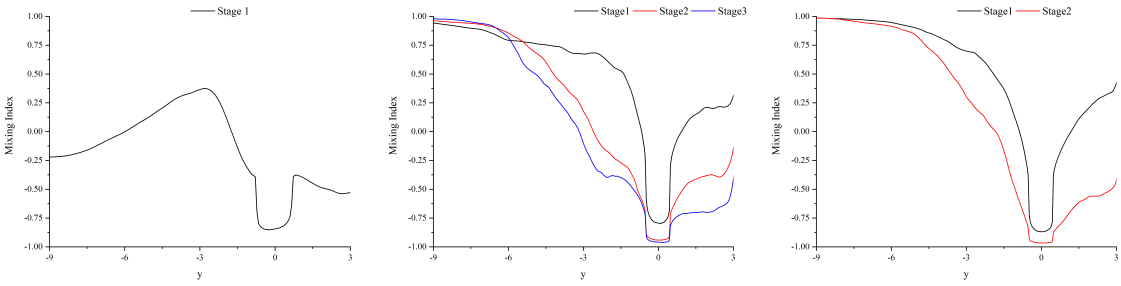

Figure 3.13: Plots of $MI2$ for Sc = 100 (a) Re = 200. (b) Re = 600. (c) Re = 1000.

For the low Schmidt number case (Sc = 1), all cases show good mixing, with $MI2$ close to 1. Also, the distribution of mixing index of all flow stages are very similar, especially for Re = 1000 case. The reason is that, at low Schmidt number cases, molecular diffusion of the scalars is more dominant which leads to more uniform mixing. In this way, both the uniformity of solution and the correlation of solution 1 and solution 2 are very high.

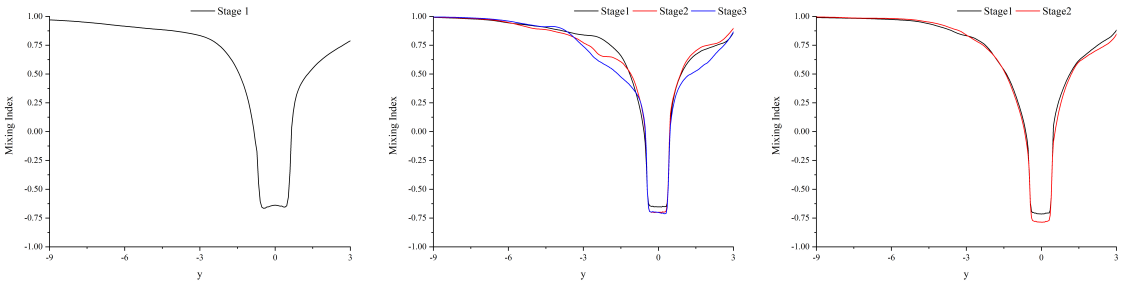

Figure 3.14: Plots of $MI2$ for Sc = 100 (a) Re = 200. (b) Re = 600. (c) Re = 1000.

3.4 Residence Time

CIJMs are not only used for the mixing of chemical species, but also the chemical reaction of solutions and particles that requires fast mixing. For instance, Santos, Mao et al [11] employed a CIJM for the chemical reaction of pDNA and polyethyleneimine (PEI) and achieved continuous production of lPEI/plasmid DNA nanoparticles. The mixing quality of CIJM is important for the chemical reaction, because better mixing can create more uniform local conditions for the reaction, and it is easier to control the size and composition of the product. In addition to local mixing condition, the uniformity of the product size and composition is also important for this kind of continuously happening chemical reaction. Note that the final product size and composition not only depend on the local mixing quality but also, the overall residence time of the reactant in the mixing chamber. Thus to achieve a uniform particle size and composition, it is also important to design for more uniform residence times in

the mixer. In the present study, we calculate the Eulerian residence time at the outlet plane of the device by the following transport equation.

$$\frac{\partial \tau}{\partial t} + \vec{\mathbf{u}} \cdot \boldsymbol{\nabla} \tau = H(\vec{\mathbf{x}}) \tag{3.4}$$

where τ is the residence time, $\vec{\mathbf{u}}$ is velocity of fluid, and $H(\vec{\mathbf{x}})$ determined the condition of residence inside the chamber; i.e. $H(\vec{\mathbf{x}}) = 1$ for locations inside the chamber and $H(\vec{\mathbf{x}}) = 0$ for locations inside the chamber.

A higher Eulerian residence time indicates that the chemical species or the particle transported by the fluid resides for a longer time inside the chamber before it exits. The underlying hypothesis here is that a fluid particle that resides longer in chamber will continue to react and grow the size of the "product" particle. Thus the size of product and composition of the nanoparticle resulting from the reaction depends directly on the residence time and so, the uniformity of the residence time or the narrow clustering of the residence time is related with the uniformity of the product size and composition.

Figure 3.15 shows the PDF of the residence time at the outlet plane of CIJM, the mean value and standard deviation is shown in Table 3.2. For the perfectly uniform product size, the PDF should only have one peak and the standard deviation should be zero. It can be observed from Figure 3.15 that the mean value of residence time increasing slightly with the Reynolds number. Because

higher Reynolds number cases have more chaotic flow motion, the fluid particles will be trapped longer in the device, and longer residence time will be achieved.

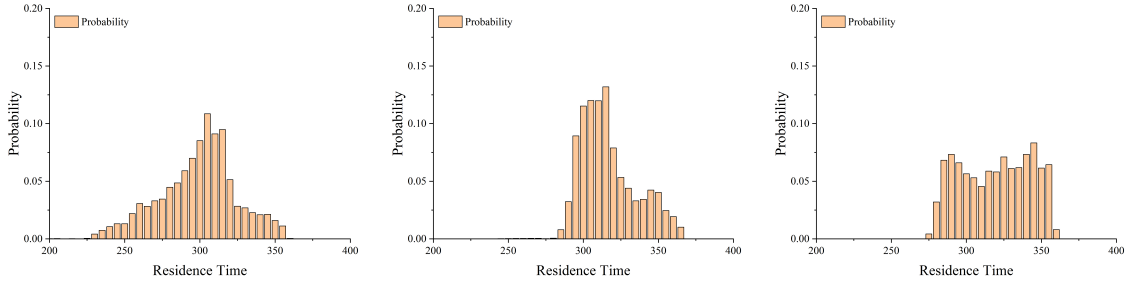

Figure 3.15: PDF of Residence Time (a) Re = 200. (b) Re = 600. (c) Re = 1000.

In terms of uniformity (narrow clustering), the Re = 600 case is better than the Re = 1000 case. A possible reason for this is that, as shown in section 3.1, the Re = 600 case has the largest amplitude of shear layer flapping, so the fluid particles will not directly goes up or down, but will be swept over each ydirection slice of the chamber. In this way, a relatively uniform distribution of residence time can be achieved at the outlet plane of CIJM. The current results indicate that the uniformity of the residence time is determined by the non-linear flow phenomena and there could be optimal flow conditions and geometric configurations to achieve more uniform residence time distribution.

Table 3.2: Statistics of Residence Time.

Re	200	600	1000
Mean value	301.26	319.08	321.98
STD	26.02	18.75	23.22

3.5 Improvement of Mixing by Pulsating Jet

To improve the mixing quality of CIJMs, we explore the use of jet pulsatility to induce an amplification of the existing instability modes in the chamber and to enhance the turbulence in the chamber. To achieve this, we employ jet with a sinusoidal velocity perturbation at the inlet of CIJMs. The temporal profile of the velocity is as follows:

$$u_1 = 1 + \alpha sin(2\pi f) \tag{3.5}$$

$$u_2 = 1 - \alpha sin(2\pi f) \tag{3.6}$$

The two impinging jets are having same oscillation frequency and amplitude, but with a counter phase of fluctuation. We expect that this will result in a fluctuating "disk" like shear layer around the impingement point. To determine a suitable the pulsation frequency, the dominant frequency of the velocity fluctuation in the conventional CIJM need to be determined. is captured by the peak counting of filtered velocity time histories. It is found however that a Fourier spectral analysis of the velocity fluctuation is not appropriate for this because of the highly stochastic nature of the fluctuations. Instead we use a peak counting method for determining the dominant time-scale in the flow.

The Strouhal number at the Y - direction center line of each Reynolds Number case is shown in Figure 3.16, the Strouhal Number is almost constant along the center line. Turbulent kinetic energy profile is also captured at the center line, the fluctuation frequency at the peak TKE position is chosen as the representative Strouhal Number for the pulsatile jet case.

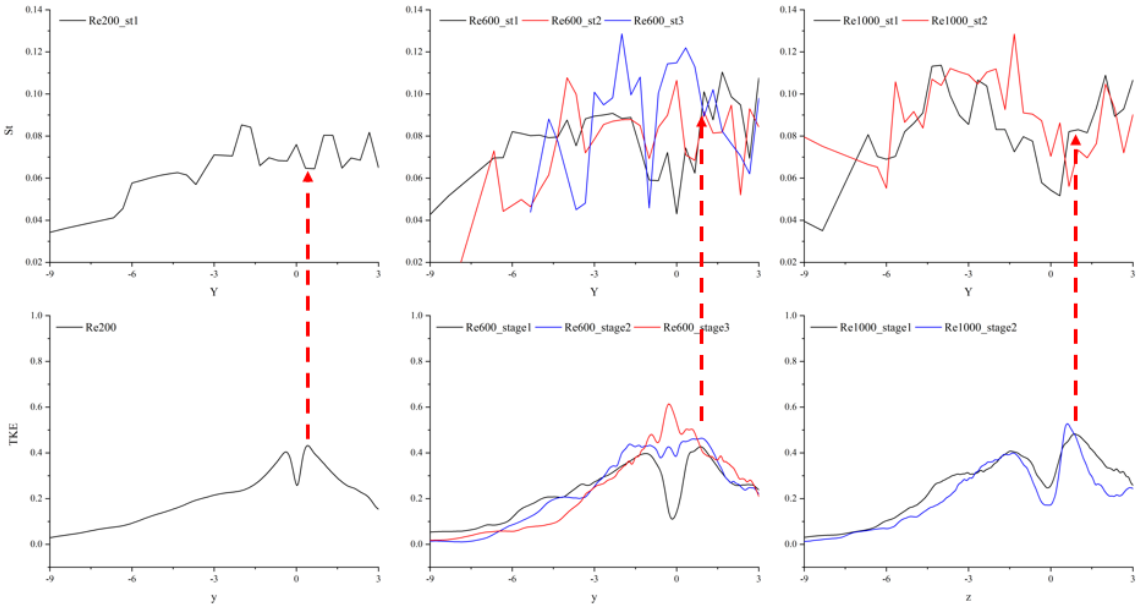

Figure 3.16: Characteristic fluctuating frequency at different locations in the CIJM determined using peak-counting of the time-variation of the velocity.

The mixing quality of CIJM with the pulsatile Jet is extracted and shown in Figure 3.17 - Figure 3.20. The result of Mixing index 1, the uniformity of chemical species is shown in Figure 3.17 and Figure 3.18. Comparing with Mixing Index of the original CIJM, the uniformity of CIJM with the pulsatile jet is slightly better than the original case, and good mixing is also reached in a closer position of the impingement point.

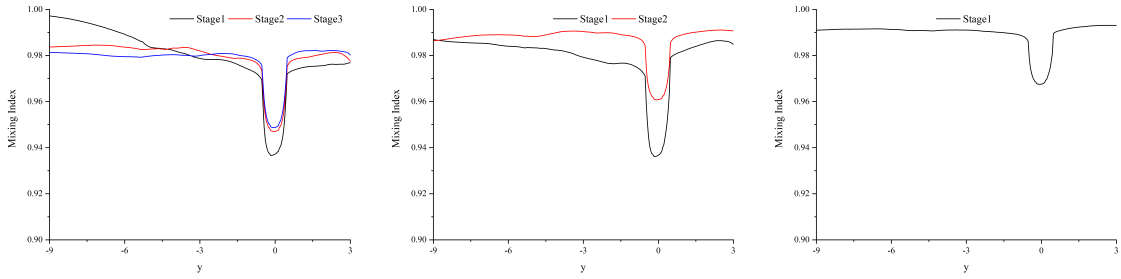

Figure 3.17: Mixing Index 1 Uniformity, Sc = 100 (a) Re = 200. (b) Re = 600. (c) Re = 1000.

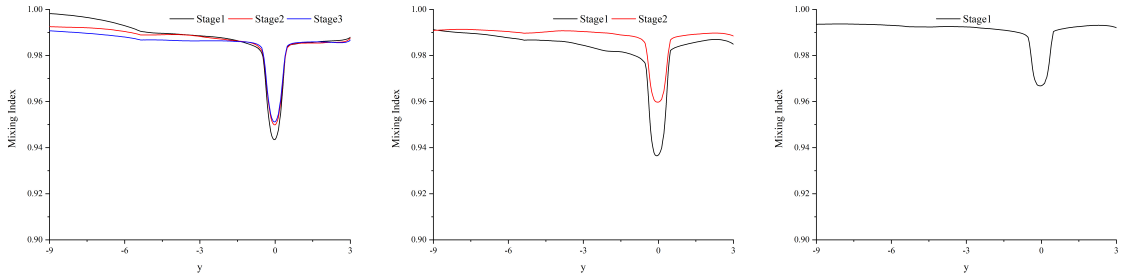

Figure 3.18: Mixing Index 1 Uniformity, Sc = 1 (a) Re = 200. (b) Re = 600. (c) Re = 1000.

The result of Mixing index 2, the cross correlation of chemical species is shown in Figure 3.19 and Figure 3.20. Comparing with the original CIJM, it can be observed that for Re = 600 and 1000 cases, the device is keep doing well on Mixing index 2. The difference is that for low Reynolds number case(Re=200), CIJM with pusatile jet can reach high quality mixing, when poor cross correlation is reached for the original case.

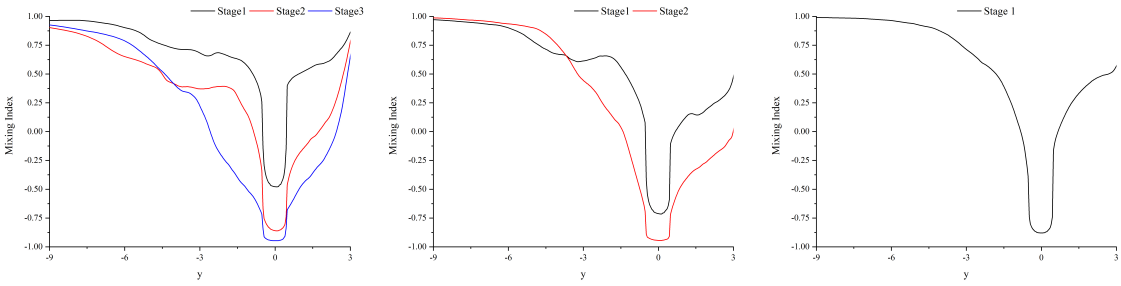

Figure 3.19: Mixing Index 2 Cross Correlation, Sc = 100 (a) Re = 200. (b) Re = 600. (c) Re = 1000.

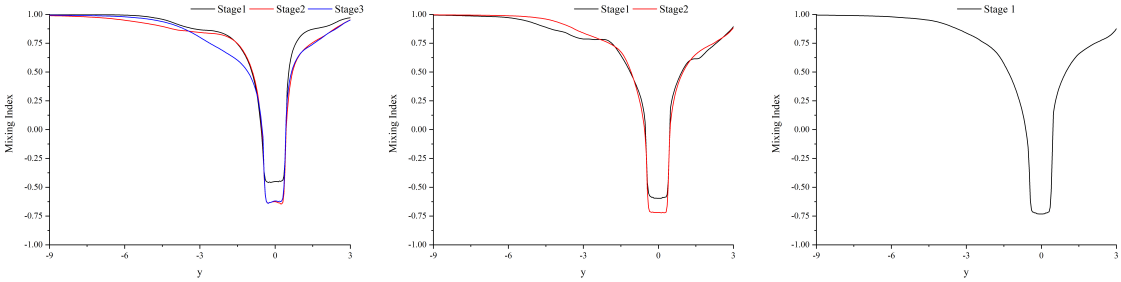

Figure 3.20: Mixing Index 2 Cross Correlation, Sc = 1 (a) Re = 200. (b) Re = 600. (c) Re = 1000.

The residence time of CIJM with pulsatile jet is shown in Figure 3.21 and the statistics of residence time is shown in Table 3.3. Comparing with the result of original CIJM, the standard deviation of all Reynolds number cases are higher, indicating that pulsatile jet makes the uniformity of residence time worse than the original case.

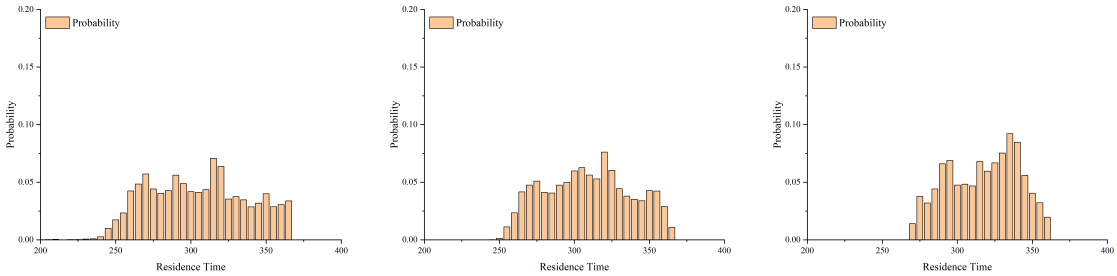

Figure 3.21: PDF of Residence Time (a) Re = 200. (b) Re = 600. (c) Re = 1000.

Table 3.3: Statistics of Residence Time.

Re	200	600	1000
Mean value	307.42	311.89	319.78
STD	32.73	28.56	23.51

In conclusion, the pulsatility in the inflow jet can improve the mixing quality, especially for low Reynolds number case but pulsatile jet can sacrifice the uniformity of the residence time.

Chapter 4

Novel Axisymmetric Confined Impinging Jet Mixer

4.1 Model description

From chapter 3, it can be observed that CIJM has good mixing quality of binary chemical species, but the uniformity of fluid residence time is diminished by the geometry of the device. The main reason for non-uniform residence time is that there are two fundamentally different path taken by fluid particle: one path is directly downwards from the impingement point to the exit, and the other path goes upwards from the impingement point and then eventually downwards to the exits. Fluid constituents that take the latter path are expected to have a higher residence time than those taking the former.

To improve the uniformity of residence time, an axisymmetrical device is proposed, which is expected to eliminate the presence of these two different fluid paths. The geometry is shown in Figure 4.1. Two jets are directly impinging at the center of the device and the outlet is the entire circumferential rim.

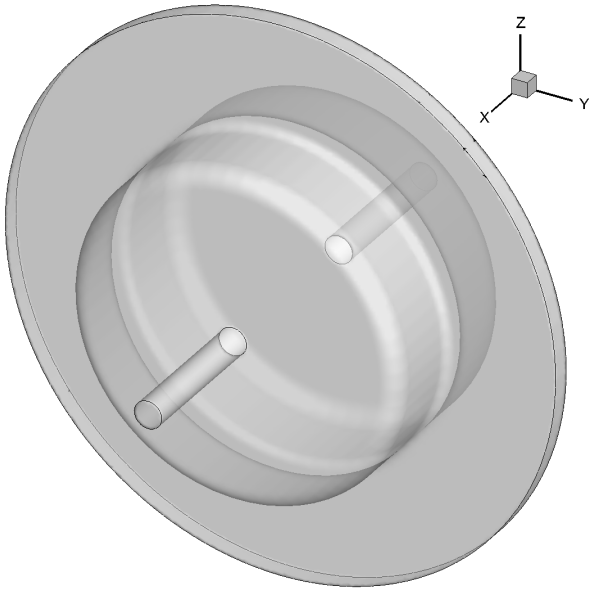

Figure 4.1: Geometry of axi-symmetrical Mixer.

4.2 Flow Field

The flow pattern of axi-symmetrical Mixer is shown in Figure 4.2 - Figure 4.4. Sub figures (a) - (d) respectively show the iso surface of the velocity magnitude, contour plot of velocity magnitude, vortical structure based on Q-criterion and contour plot of ω_z. It can be observed that for low Reynolds number cases,

the impinging jet induced shear layer is very steady, and the fluid particles are directly advecting out towards the outlet. For Re =600 and Re = 1000 case, vortical structures are formed by intrinsic instability of the impinging shear layer, but the oscillation of the shear layer is very weak.

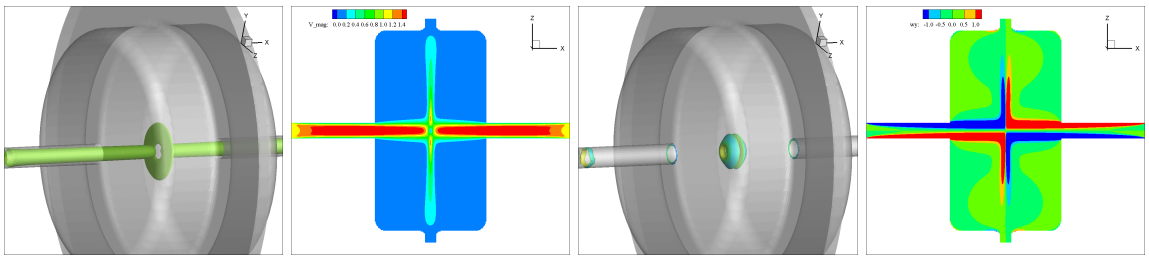

Figure 4.2: Flow Field of Re = 200 case. (a) Velocity Iso surface. (b) Velocity Contour. (c) Q-vortex Iso surface. (d) ω_z contour.

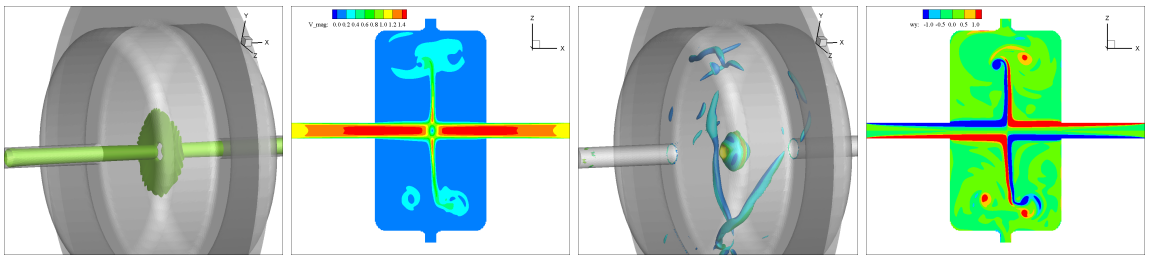

Figure 4.3: Flow Field of Re = 600 case. (a) Velocity Iso surface. (b) Velocity Contour. (c) Q-vortex Iso surface. (d) ω_z contour.

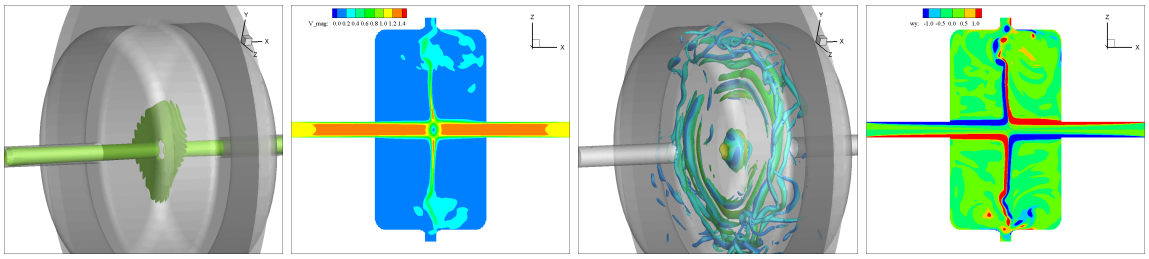

Figure 4.4: Flow Field of Re = 1000 case. (a) Velocity Iso surface. (b) Velocity Contour. (c) Q-vortex Iso surface. (d) ω_z contour.

4.3 Residence Time

The fluid residence time of axi-symmetrical mixer is extracted at the circumferential outlet. The PDF of residence time is shown in Figure 4.5 and the statistics of residence time are shown in table 4.1. The uniformity of residence time increases with the Reynolds number. Furthermore, compared with the original design, the standard deviation of residence time is much smaller, indicating a more uniform distribution of residence time.

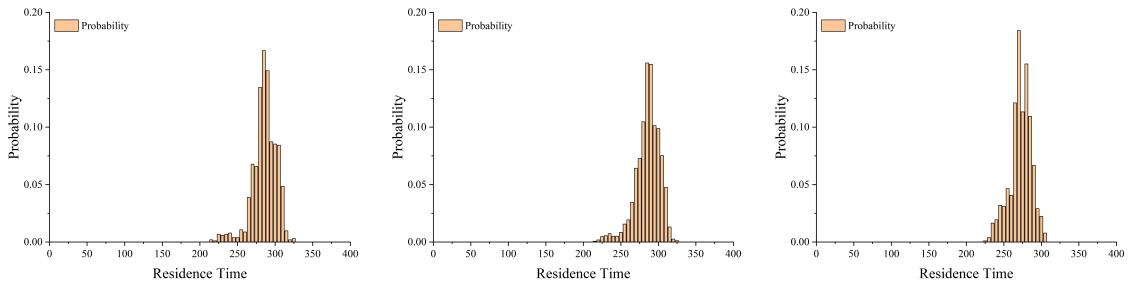

Figure 4.5: PDF of Residence Time (a) Re = 200. (b) Re = 600. (c) Re = 1000.

Table 4.1: Statistics of Residence Time.

Re	200	600	1000
Mean value	288.15	288.31	274.84
STD	16.23	16.30	14.36

4.4 Mixing Quality

The mixing quality of axi-symmetrical mixer is also evaluated at the outlet region. Table 4.2 shows the mixing quality in terms of the cross correlation of scalar 1 and scalar 2. For high Schmidt number chemical species, the Re = 200 case exhibits very poor mixing, while Re = 600 and Re = 1000 cases show mixing indices of 0.6 and 0.5. Thise are found to be much lower than

the original CIJM. Table 4.3 shows the mixing quality in terms of the spatial uniformity, and this metric is close to 1 as the original CIJM

Table 4.2: Mixing Index 1(Cross Correlation).

Sc	Re = 200	Re = 600	Re = 1000
100	-0.8894	0.6219	0.5244
1	0.9894	0.9185	0.8958

Table 4.3: Mixing Index 2(Uniformity).

Sc	Re = 200	Re = 600	Re = 1000
100	0.9987	0.9999	0.9999
1	0.9998	0.9999	0.9999

4.5 Introduction of Flow Disruptor

The above results show that axi-symmetrical mixer has better uniformity of fluid residence time, but worse mixing quality comparing with the original case. To improve the mixing quality and maintain good residence time uniformity, a ring - shape baffle is introduced inside the device at the radial direction. The baffler can disrupt flow and induce perturbation, and thus enhance the mixing.

The geometry of axial symmetric mixer with a baffle is shown in Figure 4.6. A ring shaped baffle is placed at the radial direction of impinging point to maintain the axial symmetry of the device.

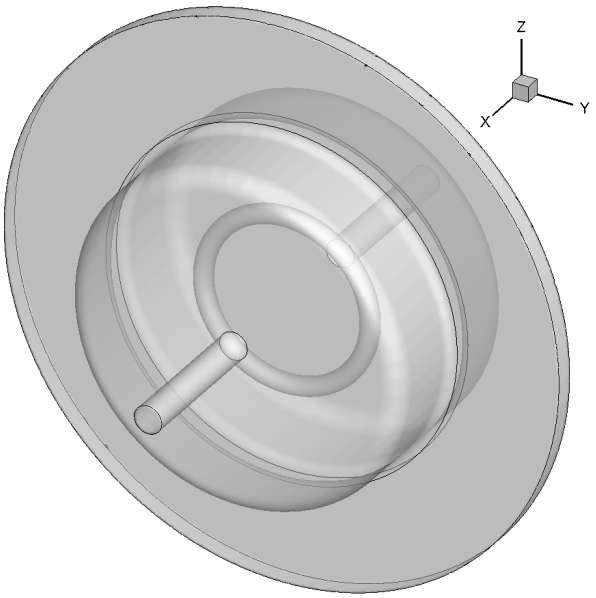

Figure 4.6: Geometry of axi-symmetrical Mixer with Baffler.

Simulations are performed for axi-symmetrical mixer with baffle at Re = 200, 600 and 1000. Figure 4.7 - Figure 4.9 shows the snap shot of the flow field of this device.

For Re = 200 and Re = 600 cases, because they have coherent flow pattern, the impinging jet induced shear layer has strong interaction with the ring shaped baffle, and the oscillation of the shear induces the complex and chaotic turbulent flow pattern in the chamber. This strong interaction and oscillation can induce fast and high quality mixing of chemical species.

For Re = 1000 case, the interaction of shear layer and ring shaped baffle occurs with the small scale structures, and the vortical structure shed by the ring are also of very small length scale.

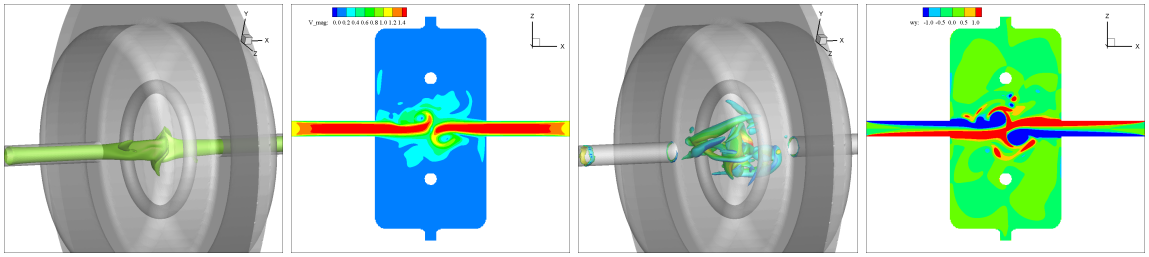

Figure 4.7: Flow Field of Re = 200 case. (a) Velocity Iso surface. (b) Velocity Contour. (c) Q-vortex Iso surface. (d) ω_z contour.

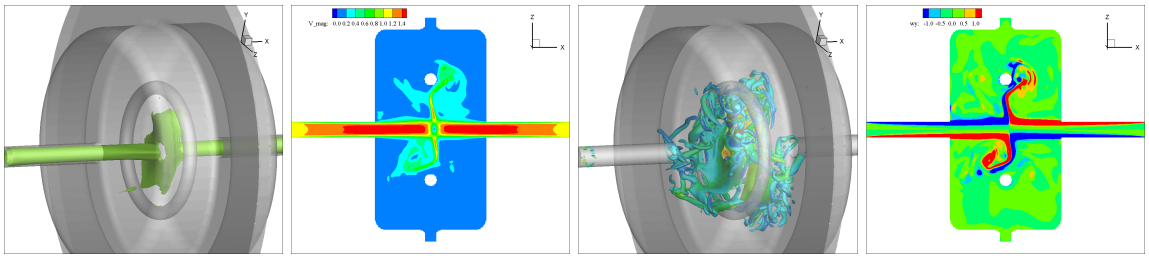

Figure 4.8: Flow Field of Re = 600 case. (a) Velocity Iso surface. (b) Velocity Contour. (c) Q-vortex Iso surface. (d) ω_z contour.

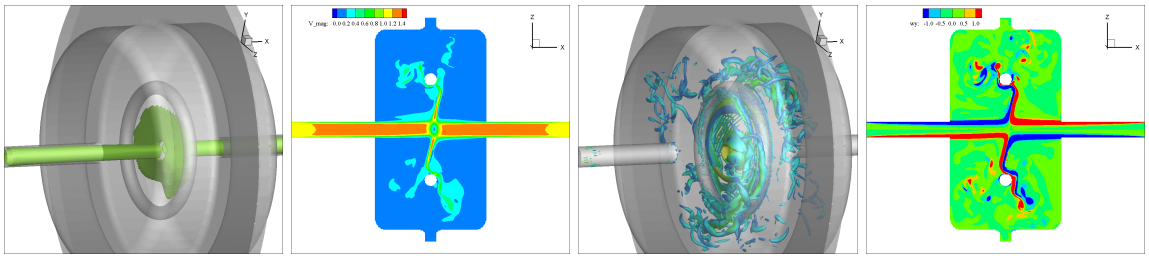

Figure 4.9: Flow Field of Re = 1000 case. (a) Velocity Iso surface. (b) Velocity Contour. (c) Q-vortex Iso surface. (d) ω_z contour.

The mixing quality of this device is extracted and mixing index 1 and mixing index 2 are respectively shown in table 4.4 and table4.5. It is observed that all cases are doing well in terms of uniformity. In terms of cross correlation, Re = 200 case and Re = 600 case has good mixing quality: mixing index 1 is around 0.9, but Re = 1000 case still has low mixing quality. The reason is that the interaction between shear layer and ring shaped baffler is with small scale structures, the amplitude of oscillation and turbulence intensity of Re = 1000 case is not as big as Re = 200 and Re = 600 case, that will resulting in a lower mixing quality.

Table 4.4: Mixing Index 1(Cross Correlation).

Sc	Re = 200	Re = 600	Re = 1000
100	0.8917	0.8812	0.5070
1	0.8865	0.9157	0.6855

Table 4.5: Mixing Index 2(Uniformity).

Sc	Re = 200	Re = 600	Re = 1000
100	0.9971	0.9995	0.9995
1	0.9989	0.9999	0.9996

Figure 4.10 shows the PDF of the distribution of residence time and table 4.6 shows the statistics of residence time. Re = 1000 case still has very uniform residence time, but the residence time distribution of Re = 200 case and Re = 600 cases become very broad banded. The standard deviation is around 30 and 25, which is similar to the original case. Considering the result of mixing index, all the cases are either doing well on mixing quality ,or uniformity of residence time, but not both.

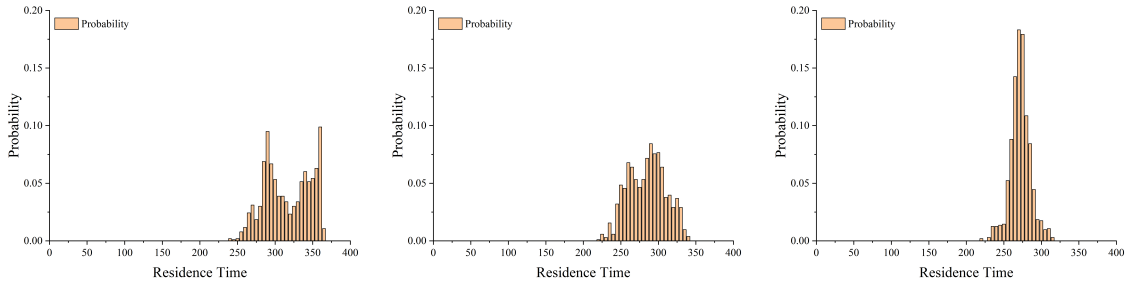

Figure 4.10: PDF of Residence Time (a) Re = 200. (b) Re = 600. (c) Re = 1000.

Table 4.6: Statistics of Residence Time.

Re	200	600	1000
Mean value	318.85	287.20	274.50
STD	30.80	24.86	13.57

Chapter 5

Conclusion

In this study, the flow pattern, turbulence characteristics, mixing quality and residence time of confined impinging jet mixers (CIJMs) have been investigated via direct numerical simulations. To study the influence of Reynolds number three cases with Reynolds numbers of 200, 600 and 1000 cases are examined. Passive transported scalars are released from the inlet of the mixer and the mixing quality is quantified by two mixing indices.

The flow pattern of CIJM is very complex; a disk like structure is formed by the impinging jest. Vortex shedding is triggered by the intrinsic instability of impinging jet and the interaction of vortical structures and the inner wall of CIJM can enhance the instability of the flow. Vortical structure can feed back to the impinging disk and the main jet, leading to low-frequency called self sustained oscillation of the jet. The averaged flow field and statistics of

flow pattern shows the most intensive fluctuation (highest TKE) happens at a position close to the impingement point and the TKE decays along the downstream direction. The result also showing that the TKE of Re = 600 case is the highest among all the cases. This case introduced large-scale movement in the jet impingement point due to large vortical motion but but for the Re = 1000 case, the vortex breaks down before it reached back on the the impinging disk and the main flow. The results show that the CIJM is a very good mixer, for Re = 600 and Re = 1000 cases the mixing quality very good both in terms of solution uniformity and cross correlation of solution concentrations. However, for Re = 200, while the uniformity of the solution concentration is good, the distribution of the two solution concentration are not similar. Consequently, the crosscorrelation metric exhibits low mixing quality. If low Schmidt number (Sc = 1) species are released, diffusion of the solution dominates the mixing and all cases show good mixing for both metrics. If chemical reaction between the two species within the CIJM is considered, the uniformity of the fluid residence time is directly related to the uniformity of the product size and composition. The PDF of the residence time shows that the Re = 600 case has the most uniform residence time, indicating that the uniformity of the residence time is determined by complex non-linear flow phenomena within the CIJM.

Appendix A

Grid Convergence Test

Grid Convergence test is performed for the simulation of CIJM. A coarser grid resolution (256 208 116) and finer grid resolution (512 388 218) is employed in addition to the baseline grid resolution (380 292 165).

The time averaged x, y and z direction velocity component are shown in Figure A.1. Results with three grid resolution of U velocity in along x centerline, V velocity in along y centerline, W velocity in along z centerline is compared, and reasonable agreement (less than 5

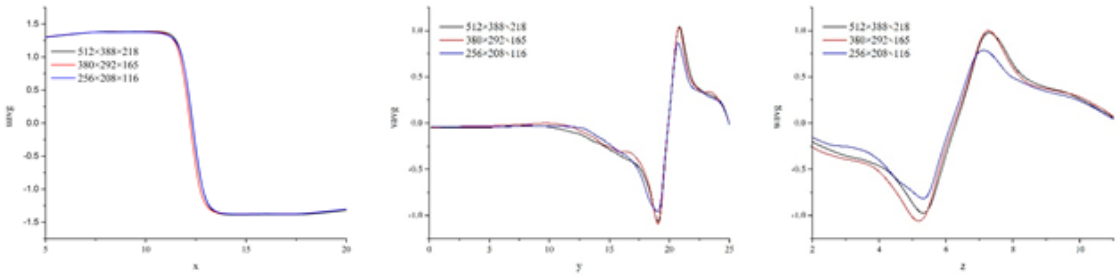

Figure A.1: Grid Convergence test (a) U avg along x - center line (b) V avg along y - center line (c) W avg along z - center line.

Bibliography

[1] J. C. Kasper, D. Schaffert, M. Ogris, E. Wagner, and W. Friess, "The establishment of an up-scaled micro-mixer method allows the standardized and reproducible preparation of well-defined plasmid/lpei polyplexes," *European Journal of Pharmaceutics and Biopharmaceutics*, vol. 77, no. 1, pp. 182–185, 2011.

[2] Q. Feng, J. Sun, and X. Jiang, "Microfluidics-mediated assembly of functional nanoparticles for cancer-related pharmaceutical applications," *Nanoscale*, vol. 8, no. 25, pp. 12 430–12 443, 2016.

[3] D. Liu, S. Cito, Y. Zhang, C.-F. Wang, T. M. Sikanen, and H. A. Santos, "A versatile and robust microfluidic platform toward high throughput synthesis of homogeneous nanoparticles with tunable properties," *Advanced Materials*, vol. 27, no. 14, pp. 2298–2304, 2015.

[4] D. Liu, H. Zhang, S. Cito, J. Fan, E. Makila, J. Salonen, J. Hirvonen, T. M. Sikanen, D. A. Weitz, and H. A. Santos, "Core/shell nanocomposites pro-

duced by superfast sequential microfluidic nanoprecipitation," *Nano letters*, vol. 17, no. 2, pp. 606–614, 2017.

[5] B. K. Johnson and R. K. Prud'homme, "Chemical processing and micromixing in confined impinging jets," *AIChE Journal*, vol. 49, no. 9, pp. 2264–2282, 2003.

[6] Y. Liu and R. O. Fox, "Cfd predictions for chemical processing in a confined impinging-jets reactor," *AIChE Journal*, vol. 52, no. 2, pp. 731–744, 2006.

[7] Y. Liu, C. Cheng, R. K. Prudhomme, and R. O. Fox, "Mixing in a multi-inlet vortex mixer (mivm) for flash nano-precipitation," *Chemical Engineering Science*, vol. 63, no. 11, pp. 2829–2842, 2008.

[8] C. E. Frouzakis, A. G. Tomboulides, J. Lee, and K. Boulouchos, "From diffusion to premixed flames in an h2/air opposed-jet burner: the role of edge flames," *Combustion and Flame*, vol. 130, no. 3, pp. 171–184, 2002.

[9] I. Valente, E. Celasco, D. Marchisio, and A. Barresi, "Nanoprecipitation in confined impinging jets mixers: Production, characterization and scale-up of pegylated nanospheres and nanocapsules for pharmaceutical use," *Chemical engineering science*, vol. 77, pp. 217–227, 2012.

[10] D. A. Johnson and P. E. Wood, "Self-sustained oscillations in opposed im-

pinging jets in an enclosure," *The Canadian Journal of Chemical Engineering*, vol. 78, no. 5, pp. 867–875, 2000.

[11] J. L. Santos, Y. Ren, J. Vandermark, M. M. Archang, J.-M. Williford, H.-W. Liu, J. Lee, T.-H. Wang, and H.-Q. Mao, "Continuous production of discrete plasmid dna-polycation nanoparticles using flash nanocomplexation," *Small*, vol. 12, no. 45, pp. 6214–6222, 2016.

[12] A. Nikoubashman, V. E. Lee, C. Sosa, R. K. Prudhomme, R. D. Priestley, and A. Z. Panagiotopoulos, "Directed assembly of soft colloids through rapid solvent exchange," *ACS nano*, vol. 10, no. 1, pp. 1425–1433, 2015.

[13] C. L. Tucker III and N. P. Suh, "Mixing for reaction injection molding. i. impingement mixing of liquids," *Polymer Engineering & Science*, vol. 20, no. 13, pp. 875–886, 1980.

[14] P. Wood, A. Hrymak, R. Yeo, D. Johnson, and A. Tyagi, "Experimental and computational studies of the fluid mechanics in an opposed jet mixing head," *Physics of Fluids A: Fluid Dynamics*, vol. 3, no. 5, pp. 1362–1368, 1991.

[15] D. R. Unger and F. J. Muzzio, "Laser-induced fluorescence technique for the quantification of mixing in impinging jets," *AIChE Journal*, vol. 45, no. 12, pp. 2477–2486, 1999.

[16] R. J. Santos, E. Erkoç, M. M. Dias, A. M. Teixeira, and J. C. B. Lopes, "Hydrodynamics of the mixing chamber in rim: Piv flow-field characterization," *AIChE Journal*, vol. 54, no. 5, pp. 1153–1163, 2008.

[17] M. Icardi, E. Gavi, D. L. Marchisio, M. G. Olsen, R. O. Fox, and D. Lakehal, "Validation of les predictions for turbulent flow in a confined impinging jets reactor," *Applied Mathematical Modelling*, vol. 35, no. 4, pp. 1591–1602, 2011.

[18] R. J. Santos, A. M. Teixeira, E. Erkoç, M. Sultan, A. M. Karpinska, M. M. Dias, and J. C. B. Lopes, "Validation of a 2d cfd model for hydrodynamics' studies in cij mixers," *International Journal of Chemical Reactor Engineering*, vol. 8, no. 1, 2010.

[19] D. L. Marchisio, "Large eddy simulation of mixing and reaction in a confined impinging jets reactor," *Computers & Chemical Engineering*, vol. 33, no. 2, pp. 408–420, 2009.

[20] C. P. Fonte, M. A. Sultan, R. J. Santos, M. M. Dias, and J. C. B. Lopes, "Flow imbalance and reynolds number impact on mixing in confined impinging jets," *Chemical Engineering Journal*, vol. 260, pp. 316–330, 2015.

[21] L. J. Lee, J. M. Ottino, W. E. Ranz, and C. W. Macosko, "Impingement mixing in reaction injection molding," *Polymer Engineering & Science*, vol. 20, no. 13, pp. 868–874, 1980.

BIBLIOGRAPHY

[22] J. Baldyga and J. Bourne, "Distribution of striation thickness from impingement mixers in reaction injection molding," *Polymer Engineering & Science*, vol. 23, no. 10, pp. 556–559, 1983.

[23] N. D. Gonçalves, H. M. Salvador, C. P. Fonte, M. M. Dias, J. C. B. Lopes, and R. J. Santos, "On the 2d nature of flow dynamics in opposed jets mixers," *AIChE Journal*, vol. 63, no. 6, pp. 2335–2347, 2017.

[24] J. Kim and P. Moin, "Application of a fractional-step method to incompressible navier-stokes equations," *Journal of computational physics*, vol. 59, no. 2, pp. 308–323, 1985.

[25] R. Mittal and G. Iaccarino, "Immersed boundary methods," *Annu. Rev. Fluid Mech.*, vol. 37, pp. 239–261, 2005.

[26] R. Mittal, H. Dong, M. Bozkurttas, F. Najjar, A. Vargas, and A. Von Loebbecke, "A versatile sharp interface immersed boundary method for incompressible flows with complex boundaries," *Journal of computational physics*, vol. 227, no. 10, pp. 4825–4852, 2008.

Yue Hao

yhao14@jhu.edu | 443-467-9310 | 3400 N Charles Street, Baltimore, MD

EDUCATION

Johns Hopkins University — Baltimore, MD
Master of Science in Mechanical Engineering; GPA: 4.0/4.0 — *Expected May 2019*

Thesis: Flow Physics and Mixing of a Confined Impinging Jet Mixer

Relevant Coursework: Fluid Dynamics I, Fluid Dynamics II; Numerical Method, Computational Fluid Mechanics, Multi-phase Flow, Turbulence Theory, Mathematical Methods for Engineering

Tsinghua University — Beijing, China
Bachelor of Engineering in Thermal Engineering; GPA: 3.50/4.0 (87/100) — *Aug 2013 - Jul 2017*

PUBLICATION

- **Hao, Y.**, Tan, L. (2018). Symmetrical and unsymmetrical tip clearances on cavitation performance and radial force of a mixed flow pump as turbine at pump mode. Renewable Energy, 127, 368-376.
- **Hao, Y.**, Tan, L., Liu, Y., Xu, Y., Zhang, J., Zhu, B. (2017). Energy performance and radial force of a mixed-flow pump with symmetrical and unsymmetrical tip clearances. Energies, 10(1), 57.
- Liu, Y., Tan, L., **Hao, Y.** Xu, Y. (2017). Energy performance and flow patterns of a mixed-flow pump with different tip clearance sizes. Energies, 10(2), 191.

PRESENTATION

- **Hao, Y.**, Seo, J. H., Hu, Y., Mao, H. Q., Mittal, R. (2018). Flow Physics and Enhanced Mixing in Confined Impinging Jet Mixers. Bulletin of the American Physical Society.
- **Hao, Y.**, Tan, L., Li, J., Wang, Y., Liu, Y. (2016) Cavitation induced radial load in a mixed-flow pump with unsymmetrical blade tip clearance. International Symposium of Cavitation and Multiphase Flow.

RESEARCH EXPERIENCE

Mechanical Engineering, Johns Hopkins University — Baltimore, MD
Research Assistant, Project: Flow Physics and Mixing of Confined Impinging Jet Mixer — *Sep 2017 - Jan 2019*

- **Advisors**: Rajat Mittal, Professor; Junhee Seo, Associate Research Professor
  - Simulated flow pattern, extracted 3D velocity and vorticial structure of Confined Impinging Jet Mixer with in-house immersed boundary DNS code (Vicar3D);
  - Analyzed mixing quality in terms of uniformity and cross-correlation and residence time in terms of uniformity;
  - Analyzed flow fluctuation frequency by spectrum, peak-counting and wavelet analysis, analyzed the contributing factor of fluctuation frequency by simulating unconfined impinging jet mixer;
  - Analyzed mixing length scale by calculating spatial spectrum of concentration field;
  - Improved mixing quality by implementing pulsating impinging jet with dominant frequency of fluctuation;
  - Improved Particle Laden Flow solver by adding drag and lift into particle moving functions (subroutine);
  - Implemented convection diffusion scalar transport solver and particle laden flow solver into graph-partition version of group in-house code (Vicar3D).

Thermal Engineering, Tsinghua University — Beijing, China
Research Assistant, Project: Research of tip leakage flow and radial force of mixed flow pump — *May 2015 - Jul 2017*

- **Advisors**: Shuliang Cao, Professor; Lei Tan, lecturer
  - Simulated the flow pattern of mixed flow pump with RNG k-Îţ turbulence model in ANSYS CFX and captured the characteristics of new born, fall off and development of tip leakage vortex by extracting the streamline and iso-surface of Q-vortex around the tip clearance;
  - Simulated the generation and development of cavitation bubble by Zwart-Gerber-Belamri model in ANSYS CFX, calculated energy performance of pump as function of NPSH;
  - Analytically calculated the frequency of radial force caused by rotor stator interaction, compared with computational result from simulation and experimental result from literature;
  - Monitored the radial force on principal axis, analyzed the transient characteristic of radial force by orbit plot, time domain and frequency domain analysis.

Mechanical Engineering, Georgia Institute of Technology — Georgia, USA
Research Assistant, Project: Thrombus prediction in centrifugal pump — *May 2016 - Sep 2016*

- **Advisor**: David Ku, Professor
  - Designed a centrifugal pump in clinical and in vitro circuits based on model of Sorin Pump by bladegen, considered the shape of blade, hub and shroud to achieve high hydraulic performance;

- Calculated shear rate distribution in centrifugal pumps using SST k-ÏĽ turbulence model in ANSYS CFX, analyzed correlation of low shear rate region and thrombosis region;
- Analyzed the cause of low shear rate section and the relationship with pin size, gap height and rotation speed; improved the design of pump to reduce the area of low shear rate section.

Thermal Engineering, Tsinghua University Beijing, China

Group Leader, Project: Improvement of thermal conductivity measurement *Feb 2015 - May 2015*

- **Advisor**: Hui Li, associate research scientist
  - Analyzed the system error of constant power plane heat source method measuring heat conductivity by literature review, mathematical deduction and numerical simulation, focused on the system error caused by heat capacity of heating piece;
  - Investigated the heat conduction process with surface heat transfer analytically and simulated the process of heat transfer numerically with MATLAB;
  - Fitted an empirical formula calculating the exact value of heat conductivity by the global optimal algorithm, experimentally validated the formula;

HONORS AND AWARDS

- Outstanding Bachelor thesis of Tsinghua University,1/20
- Comprehensive scholarship-Weichai Power scholarship, 3/83
- First Price of Outstanding SRT, 1/30
- Five star volunteer of Tsinghua University

SKILL HIGHLIGHTS

- Commercial Software: Fluent, CFX, Tecplot, CFD-Post, ICEM, Turbogrid, Simens NX, Solidworks, AutoCAD